Journal of Solid State Chemistry **142,** 51–56 (1999)
Article ID jssc.1998.7984, available online at http://www.idealibrary.com on IDEAL®

Substitution of Mg^{2+} and Fe^{2+} in the Trigonal-Bipyramidal-Coordinated Site in β''-(Mg, Fe)$Al(PO_4)O$

St. Knitter

Institut für Anorganische Chemie, Universität Hannover, D-30167 Hannover, Germany

and

P. Schmid-Beurmann[1] and L. Cemič

Mineralogisch Petrographisches Institut, Christian Albrechts Universität Kiel, D-24098 Kiel, Germany

Received March 26, 1998; in revised form July 29, 1998; accepted August 2, 1998

Solid solution compositions in the system $FeAl(PO_4)O$–$MgAl(PO_4)O$ were synthesized hydrothermally at 735°C and 0.2 GPa and controlled oxygen fugacities. X-ray powder diffraction studies reveal that under these conditions a complete solid solution series is formed. It is characterized by the substitution of Mg^{2+} and Fe^{2+} in a fivefold-coordinated trigonal-bipyramidal site. The solid solution compositions are isotypic with the end members, having the β''-$MgAl(PO_4)O$ structure, and crystallize in the monoclinic space group $P2_1/c$. ^{57}Fe-Mössbauer spectroscopic measurements show that these phases are paramagnetic at room temperature. They are characterized by an isomer shift between 1.18 and 1.20 mm/s relative to α-iron and a compositionally dependent quadrupole splitting between 2.52 and 2.61 mm/s for high-spin $^{57}Fe^{2+}$ in the trigonal-bipyramidal-coordinated Me^{2+} site.

INTRODUCTION

Mg^{2+} or Fe^{2+} in trigonal-bipyramidal coordination occurs only seldomly in solid compounds. It has been recognized in the iron phosphates $Fe_7(PO_4)_6$ (1), $Fe_7(P_2O_7)_4$ (2), and $Fe_4(PO_4)_2O$ (3), the minerals grandidierite [(Mg,Fe)Al_3SiBO_9] (4), wagnerite [$Mg_2(PO_4)F$] (5), althausite [$Mg_2(PO_4)$(OH,F)] (6), and farringtonite [$Mg_3(PO_4)_2$] (7), synthetic graftonite [$Fe_3(PO_4)_2$] (8), and the wolfeite–triploidite series [$(Fe,Mn)_2(PO_4)$(OH,F)] (9). With the exception of grandidierite and the title compounds, Mg or Fe^{2+} occupies more than one crystallographic position in the structures of the above-mentioned phases. No natural or synthetic Fe^{2+} end member of the grandidierite series has been synthesized or found in natural environments. The solid solution series $(Mg_{1-x},Fe_x^{2+})_3(PO_4)_2$ was investigated by Annersten *et al.* (10) in the compositional range $0 \le x \le 0.6$. At higher Fe concentrations a miscibility gap is present in this system, because the Fe^{2+} and the Mg end members are not isotypic. Therefore, the $(Mg_{1-x},Fe_x)Al(PO_4)O$ solid solution represents the only known compound which offers the opportunity to investigate the crystal chemical behavior of Mg and Fe^{2+} along a complete solid solution series.

Here we report the synthesis and an investigation of the lattice parameters and Mössbauer spectroscopic properties of the $(Mg_{1-x},Fe_x)Al(PO_4)O$ series.

PREVIOUS WORK

$MgAl(PO_4)O$ was originally prepared (11) from MgO, $Al(OH)_3$ (gibbsite), and $(NH_4)H_2PO_4$ between 900 and 1350°C. The synthesis was performed in air at ambient pressure. It was argued from DTA measurements that $MgAl(PO_4)O$ is present in the temperature range between 193 and 1050°C in five different modifications: $\alpha \leftarrow 1050°C \rightarrow \alpha' \leftarrow 485°C \rightarrow \beta \leftarrow 259°C \rightarrow \beta' \leftarrow 193°C \rightarrow \beta''$.

The α-, α′-, β-, and β′-phases were not quenchable and at room temperature only the β″-modification was detected (11). In hydrothermal experiments β″-$MgAl(PO_4)O$ and $FeAl(PO_4)O$ were identified as decomposition products of synthetic lazulite [$MgAl_2(OH)_2(PO_4)_2$] and scorzalite [$FeAl_2(OH)_2(PO_4)_2$] (12, 13).

$FeAl(PO_4)O$ and β″-$MgAl(PO_4)O$ were found to be isotypic, both having the monoclinic space group $P2_1/c$ (14, 15). Their structure contains AlO_4 tetrahedra which form single chains with the periodicity of two tetrahedra along the crystallographic *c*-direction (Fig. 1a). These chains are connected with each other via isolated PO_4 tetrahedra. Mg^{2+} and Fe^{2+} occupy a single crystallographic position, which is surrounded by oxygen in the

[1] To whom correspondence should be addressed.

0022-4596/99 $30.00

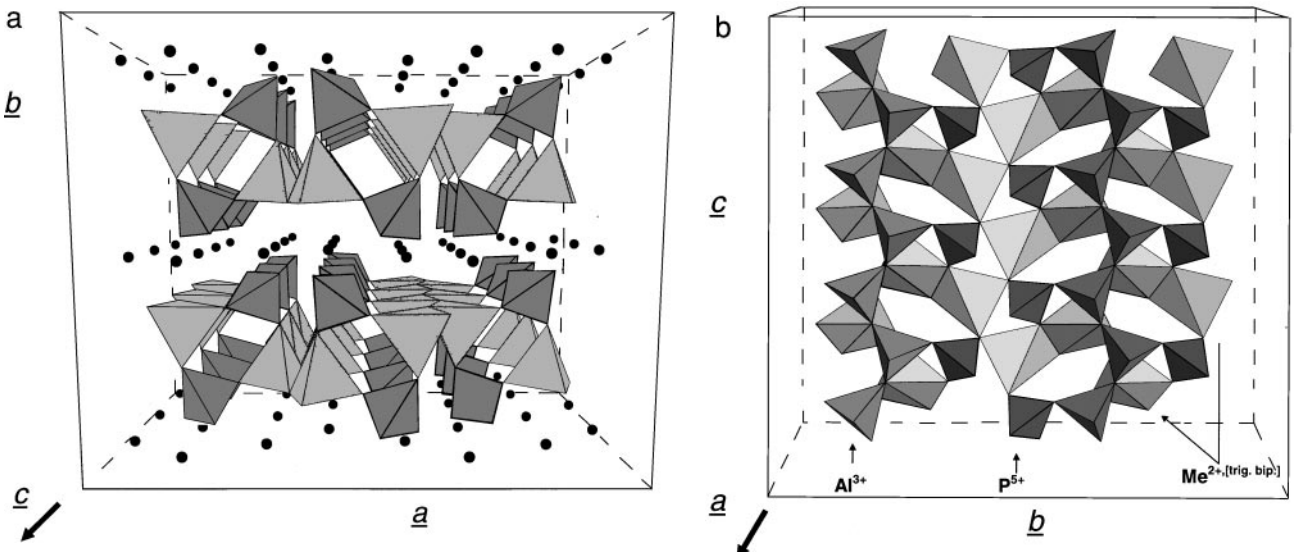

FIG. 1. View along (a) the *c*-direction and (b) the *a*-direction of the crystal structures of $FeAl(PO_4)O$ and β''-$MgAl(PO_4)O$, respectively (14, 15). Al^{3+} are represented by bright tetrahedra, and P^{5+} by dark tetrahedra. In (a) Me^{2+} are shown as spheres and in (b) as edge-sharing trigonal bipyramids (fivefold coordination).

form of a trigonal bipyramid. Two of these polyhedra are connected via edges to form small clusters. These are linked to four surrounding bipyramids via common corners to form a two-dimensional net (Fig. 1b). These Me^{2+} sites are separated from each other in the *b*-direction by the layers formed by the tetrahedral Al_2O_6 chains and the connecting PO_4 tetrahedra.

EXPERIMENTAL

Synthesis

Different compositions of the $(Mg,Fe)Al(PO_4)O$ solid solution series were synthesized in steps of 12.5 mol% using standard hydrothermal buffer techniques. As starting materials, MgO (Merck no. 5865, p.a.), Fe (Merck no. 819, p.a.), Fe_2O_3 (Merck no. 3924), and α-$AlPO_4$ (berlinite) were used. α-$AlPO_4$ was synthesized from γ-Al_2O_3 and H_3PO_4 (Merck no. 573, p.a.) with a small excess of orthophosphoric acid at 0.3 GPa and 500°C for 3 days. γ-Al_2O_3 was used instead of the less reactive α-Al_2O_3 (corundum). It was prepared by dissolving Al ribbon (Merck no. 1057, p.a.) in HCl and by subsequent heating of the precipitate at temperatures slightly below 1000°C for 10 min. The starting compounds for the synthesis of the $(Mg,Fe)Al(PO_4)O$ solid solution compositions were weighed in the appropriate proportions and homogenized in a mortar. Between 50 and 100 mg of sample was sealed in Ag/Pd tubes together with 20 µl of distilled water. The Ag/Pd tubes were then placed, together with 200 mg of powdered Ni/NiO buffer and 30 µl of distilled water, into larger Au capsules which were then sealed. The experiments were carried out in a conventional hydrothermal apparatus with horizontally arranged Tuttle-type cold-seal bombs at $T = 735$°C and $P = 0.2$ GPa. The temperature was controlled using Ni–CrNi thermocouples. The overall uncertainty in temperature was estimated to be less than ± 3°C. The pressure was measured with a Heise gauge, and as it could not be read better than ± 2.5 MPa, this was considered to be the uncertainty in pressure. An experiment was ended by switching off the power. The autoclaves were then cooled in a cold air stream. Room temperature was attained within 0.5 h. The experiment durations were 9 days.

X-Ray Powder Diffraction

X-ray powder diffraction was used for phase characterization [Siemens D5000 powder diffractometer with Cu$K\alpha$ radiation and a secondary graphite -(001) monochromator (operation conditions: 40 kV, 20 mA)]. The unit cell parameters were refined from the peak positions using the least-squares program PULVER91 (16).

^{57}Fe-Mössbauer Spectroscopy

Mössbauer spectra were recorded at room temperature using a $\sim$1-GBq $^{57}Co/Rh$ source in combination with a constant-acceleration spectrometer. For absorber preparation the $(Mg_{1-x},Fe_x)Al(PO_4)O$ samples were diluted with sugar as a matrix and pressed into pellets with a diameter of 0.5 in. This procedure resulted in absorber densities between 3 and 5 mg of Fe/cm^2. The spectra were calibrated with an α-Fe foil. Pure Lorentzian line shapes with variable line width (FWHM) were fitted to the spectra.

RESULTS

Characterization of the β''-$(Mg_{1-x},Fe_x)Al(PO_4)O$ Solid Solution Series

The reaction products consisted of colorless crystals with sizes less than 10 μm. Most crystals showed an irregular shape with the exception of a few individuals with well-developed crystal faces. Corundum (α-Al_2O_3), farringtonite [$(Mg,Fe)_3(PO_4)_2$], and berlinite were found to be present in minor amounts by X-ray powder diffraction. The amounts were estimated as 2 wt% of corundum, 2.5 wt% of farringtonite, and 0.5–1 wt% of berlinite by quantitative phase analysis using the Rietveld method. As the partitioning of magnesium and iron between $(Mg_{1-x},Fe_x)_3(PO_4)_2$ and β''-$(Mg_{1-x},Fe_x)Al(PO_4)O$ has an influence on the composition of the latter compound, we made an effort to estimate the composition of the farringtonite phase. We determined this from the position of the $(11\bar{1})$ reflection in the powder diffraction pattern using a calibration curve which was calculated from the lattice constants given by Annersten *et al.* (10). We found that generally the farringtonite phase was enriched in the Mg component relative to the bulk composition of the run. Therefore the coexisting β''-$(Mg_{1-x},Fe_x)Al(PO_4)O$ phase should be enriched in Fe. For example, for the bulk composition with $x = Fe/(Fe + Mg) = 0.250$, $(Mg_{1-x},Fe_x)_3(PO_4)_2$ was found to have $x = 0.15$. Using the measured weight fractions, we calculated for this sample a composition of $x = 0.255$ for the coexisting β''-$(Mg_{1-x},Fe_x)Al(PO_4)O$ phase. Hence, the composition of this phase differs by the amount $\Delta x = 0.005$ from the bulk composition. Analogously we calculated the compositional data for the members of the β''-$(Mg_{1-x},Fe_x)Al(PO_4)O$ series of the other runs in Tables 1 and 2 if impurity phases were detected in the products.

TABLE 1
Lattice Constants and Molar Volume of the β''-$(Mg_{1-x},Fe_x)Al(PO_4)O$ Solid Solution Series ($Z = 4$)

x_{bulk}	x^a	a (Å)	b (Å)	c (Å)	β (deg)	V_m (10^{-6} m^3/mol)
0.000	0.000	7.1012(3)	10.347(1)	5.4421(3)	98.348(5)	59.57(4)
0.125	0.128	7.1030(5)	10.368(2)	5.4475(4)	98.296(6)	59.76(5)
0.250	0.255	7.1082(6)	10.397(2)	5.4538(4)	98.236(7)	60.05(6)
0.375	0.382	7.1119(4)	10.420(2)	5.4580(4)	98.168(6)	60.28(5)
0.500	0.505	7.1158(8)	10.449(4)	5.4640(7)	98.12(1)	60.55(9)
0.625	0.632	7.1169(6)	10.470(2)	5.4689(4)	98.066(8)	60.74(7)
0.750	0.757	7.1202(5)	10.494(2)	5.4739(4)	98.023(7)	60.97(6)
0.875	0.875	7.1207(3)	10.506(1)	5.4760(3)	97.963(4)	61.08(3)
1.000	1.000	7.1223(5)	10.532(2)	5.4804(5)	97.91(1)	61.30(9)

Note. V_m = molar volume; uncertainties = 1σ. $x = Fe/(Fe + Mg)$; x_{bulk} = bulk composition of the synthesis run.

[a] Value corrected for Mg–Fe fractionation between coexisting β''-$(Mg_{1-x},Fe_x)Al(PO_4)O$ and $(Mg_{1-x},Fe_x)_3(PO_4)_2$ (farringtonite).

TABLE 2
^{57}Fe-Mössbauer Parameters at Room Temperature of the β''-$(Mg_{1-x},Fe_x)Al(PO_4)O$ Solid Solution Series

x	IS (mm/s)	QS (mm/s)	Γ (mm/s)
0.128	1.186(3)	2.607(9)	0.25(2)
0.255	1.185(3)	2.586(10)	0.23(2)
0.382	1.179(20)	2.57(6)	0.24(13)
0.505	1.192(4)	2.581(11)	0.25(2)
0.632	1.191(3)	2.573(9)	0.27(2)
0.757	1.193(4)	2.559(11)	0.26(2)
0.875	1.190(2)	2.539(7)	0.24(1)
1.000	1.187(13)	2.523(41)	0.27(10)

Note. IS = isomer shift relative to α-iron; QS = quadrupole splitting; Γ = full width at half-maximum; uncertainties = 1σ.

Lattice Constants

The diffractograms of the solid solutions were indexed starting with the monoclinic unit cell parameters of the isotypic $FeAl(PO_4)O$ and β''-$MgAl(PO_4)O$ end members (14, 15). The results of the lattice constant refinement are shown in Fig. 2 and listed in Table 1. The lattice parameters

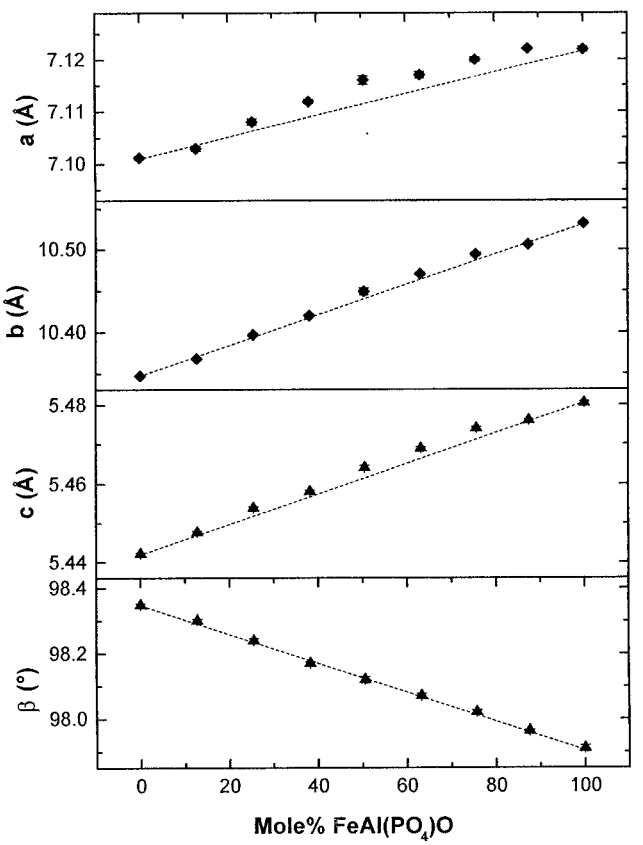

FIG. 2. Lattice parameters of members of the β''-$(Mg_{1-x},Fe_x)Al(PO_4)O$ solid solution series.

change continuously with composition. The line profiles of the reflections do not show any peak doubling or line broadening. Consequently, it can be stated that a complete solid solution is formed between β''-$MgAl(PO_4)O$ and $FeAl(PO_4)O$ at 735°C and 0.2 GPa.

^{57}*Fe-Mössbauer Spectroscopy*

^{57}Fe-Mössbauer spectra were recorded for the complete $(Mg_{1-x},Fe_x)Al(PO_4)O$ solid solution series in compositional steps of 12.5 mol%. The Mössbauer parameters are presented in Table 2. The Mössbauer spectrum of the composition with $x = 0.5$ is shown in Fig. 3. At room temperature the phases are paramagnetic and their spectra are characterized by a single quadrupole split doublet with an isomer shift (IS) of 1.19 $\pm$ 1 mm/s, which is typical for high-spin Fe^{2+} (17), and a quadrupole splitting (QS) between 2.52 and 2.61 mm/s. Hence, the well-defined doublet of Fig. 3 can unambiguously be assigned to Fe^{2+} in the trigonal-bipyramidal-coordinated site of the β''-$MgAl(PO_4)O$ structure (Fig. 1b).

DISCUSSION

The substitution of Fe^{2+} and Mg^{2+} in a trigonal-bipyramidal-coordinated site has already been investigated by Annersten *et al.* (10) with the example of the incomplete solid solution series $(Mg_{1-x},Fe_x)_3(PO_4)_2$. A miscibility gap between a Mg-rich member of farringtonite type and an Fe-rich member of graftonite type appears at Fe contents higher than $x = 0.6$. In the structure of these $(Mg_{1-x},Fe_x)_3(PO_4)_2$ phases, the metal ions are distributed over two crystallographic positions $M1$ and $M2$, which are fivefold and sixfold coordinated, respectively. In contrast to the situation, in the structure of the β''-$(Mg_{1-x},Fe_x)Al(PO_4)O$ series, only one metal position is available. Therefore, the variations of the crystal chemical properties can unequivocally be attributed to Mg^{2+}–Fe^{2+} substitution on a single site.

The a, b, and c unit cell parameters increase, starting from pure β''-$MgAl(PO_4)O$ with increasing Fe content, whereas the monoclinic angle β decreases slightly (Fig. 2). In this plot, a straight line is drawn between the end members to emphasize the deviations from Vegard's rule. This is the case for the a, b, and c unit cell parameters.

The ^{57}Fe-Mössbauer parameters of the β''-$(Mg_{1-x},Fe_x)Al(PO_4)O$ solid solutions series are plotted in Fig. 4. The

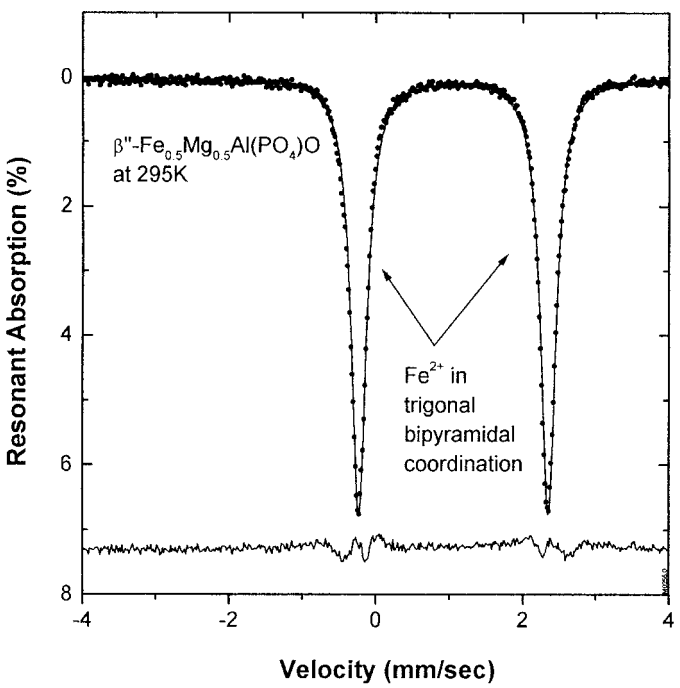

FIG. 3. Room temperature ^{57}Fe-Mössbauer spectrum of β''-$(Mg_{1-x},Fe_x)Al(PO_4)O$ with $x = 0.50$.

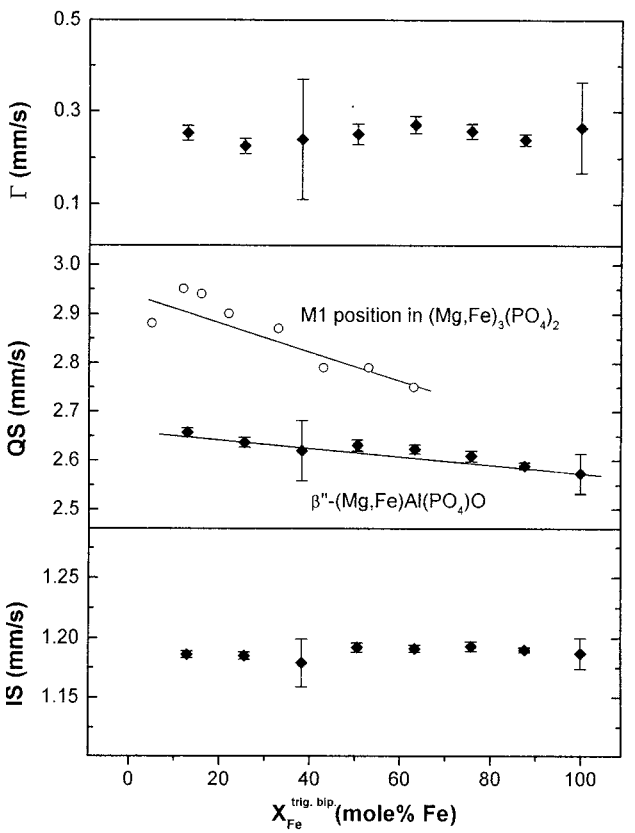

FIG. 4. Room temperature ^{57}Fe-Mössbauer parameters of trigonal-bipyramidal-coordinated Fe^{2+} in β''-$(Mg,Fe)Al(PO_4)O$ (diamonds) and $(Mg,Fe)_3(PO_4)_2$ (open circles) (10) vs $x_{Fe}^{tr.bip}$, which equals the molar ratio of Fe in the trigonal-bipyramidal site. (IS = isomer shift relative to α-Fe; QS = quadrupole splitting, Γ = full width at half-maximum.)

isomer shift does not change significantly as a function of composition. A similar situation was found for the five fold-coordinated site in $(Mg,Fe)_3(PO_4)_2$ (10). This constancy of the isomer shift indicates similar bonding properties for the trigonal-bipyramidal-coordinated Fe^{2+} over the entire range. The line width (Γ) also was found to be independent of composition. Therefore, the variation of the distribution of the electrical field gradient, V_{ZZ}, due to differing individual chemical environments of the ^{57}Fe nuclei can be taken as negligible.

The quadrupole splitting decreases significantly with increasing Fe content in the trigonal-bipyramidal-coordinated site. To examine this behavior, we considered the geometry of this site as a function of the distortion from a regular trigonal bipyramid. To quantify the distortion of a polyhedron, several indices have been defined. MacKenzie and Meinhold (18) calculated the index DI to describe the distortion of the trigonal-bipyramidal coordination around the Al^{3+} and the (Mg^{2+},Fe^{2+}) position in grandidierite $[(Mg,Fe)Al_3SiBO_9]$ with the expression

$$\mathrm{DI}_{\mathrm{tr.bip}} = \left(\sum_i^N |\theta_i^{\mathrm{obs}} - \theta_i^{\mathrm{id}}|\right) \Big/ \left(\sum_i^N \theta_i^{\mathrm{id}}\right). \qquad [1]$$

In Eq. [1] θ_i^{obs} and θ_i^{id} are the observed and the undistorted (ideal) angles. In the case of a perfect octahedron ($N = 12$), for example, all angles θ_i^{id} are equal to 90°. In the case of an ideal trigonal bipyramid ($N = 10$), six of the angles θ_i^{id} are 90°, three of them have the value of 120°, and one angle (between the apical oxygens) is 180°.

The elongation or compression of bond lengths can be described using the α parameter (19). Like the DI, this parameter was initially defined for octahedral coordination but can also be applied to the trigonal-bipyramidal coordination:

$$\alpha_{\mathrm{tr.bip.}} = \sum_i^5 |\ln(l_i/l_{\mathrm{m}})|. \qquad [2]$$

In Eq. [2] l_i is the measured and l_{m} is the mean bond length.

In Table 3 the values of the distortion parameters $\alpha_{\mathrm{tr.bip.}}$ and $\mathrm{DI}_{\mathrm{tr.bip.}}$ are given. The angular distortions of the $Me^{2+}O_5$ trigonal bipyramids of the end members β''-$MgAl(PO_4)O$ and $FeAl(PO_4)O$ expressed by the parameter $\mathrm{DI}_{\mathrm{tr.bip.}}$, are very similar. Greater differences are present in the distortion of the bond lengths, expressed by the parameter $\alpha_{\mathrm{tr.bip.}}$ This can be realized from a comparison of the Me^{2+}–O bond lengths in both compounds (Table 3) because the bond length in $FeAl(PO_4)O$ shows a greater variation. The bond length distortion of the Jahn–Teller ion Fe^{2+} in $FeAl(PO_4)O$ is much stronger than that of the Mg^{2+} ion in β''-$MgAl(PO_4)O$. Therefore, the coordination polyhedron of Fe^{2+} in $FeAl(PO_4)O$ can be considered to be more distorted than that of Mg^{2+} in β''-$MgAl(PO_4)O$. It can be expected that the distortion of the Me^{2+} coordination will also change continuously because the unit cell parameters change continuously with composition (Fig. 2). Therefore increasing distortion can be expected along the solid solution series with increasing $FeAl(PO_4)O$ content. Hence the decrease of QS with composition (Fig. 4) is correlated to an increasing distortion of the trigonal-bipyramidal coordination around the Fe^{2+} ions.

The same relation was found to be valid for members of the solid solution series of farringtonite type between $Mg_3(PO_4)_2$ and $(Mg_{0.40}Fe_{0.60})_3(PO_4)_2$ (10). In the latter system, the QS of the trigonal-bipyramidal-coordinated site

TABLE 3

Distortion Indices $\alpha_{\mathrm{tr.bip.}}$ and $\mathrm{DI}_{\mathrm{tr.bip.}}$ of Trigonal Bipyramidal Sites and Me^{2+}–O Bond Lengths in β''-$MgAl(PO_4)O$ and $FeAl(PO_4)O$

	β''-$MgAl(PO_4)O$	$FeAl(PO_4)O$
$\alpha_{\mathrm{tr.bip.}}$	0.067	0.136
$\mathrm{DI}_{\mathrm{tr.bip.}}$	0.105	0.101
	Me^{2+}–O bond lengths (Å)	
	2.022	2.045
	2.058	2.112
	2.108	2.115
	2.030	2.017
	2.080	2.187
Average	2.06(4)	2.10(7)

Note. data calculated from Refs. (14) and (15); uncertainties = 1σ.

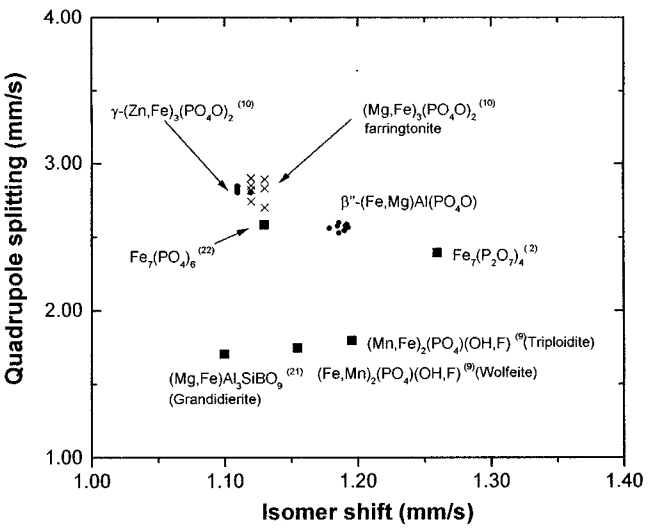

FIG. 5. Plot of quadrupole splitting vs isomer shift (relative to α-Fe) for iron in trigonal-bipyramidal coordination in various phosphates. Full circles and crosses: members of solid solution series.

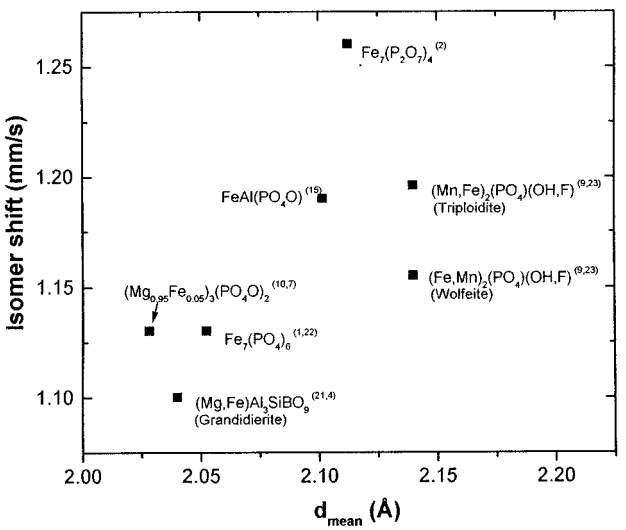

FIG. 6. Correlation of the ^{57}Fe isomer shift to the mean bond length of trigonal-bipyramidal-coordinated sites in phosphates.

also decreases with increasing Fe^{2+} concentration (Fig. 4). This was interpreted as the effect of an increasing lattice distortion in analogy to the situation of high-spin Fe^{2+} in a distorted octahedral coordination. For the latter case, Ingalls (20) has shown that the QS increases for small distortions up to a maximum value and then decreases again. Generally a QS arises when a nonzero electrical field V_{ZZ} gradient is present at the ^{57}Fe nuclei. V_{ZZ} can be split up into a lattice and a valency contribution, both having opposite sign in the case of near-octahedral coordination (20). Hence, our results and those of Annersten *et al.* (10) suggest that the same relationship between lattice and valency contribution to the electric field gradient and the QS is valid in the case of trigonal-bipyramidal coordination and in the case of octahedral coordination.

Figure 5 compares the quadrupole splitting and the isomer shift values of the β''-(Mg,Fe)Al(PO_4)O solid solution series with other phosphates which contain Fe in trigonal-bipyramidal coordination. The hyperfine parameters of the title compound fall within the range defined by the other phosphates. Furthermore, their changes, which are due to the compositional variation, are small when compared to the differences between the different phosphates. This is shown by the data points of the β''-(Mg,Fe)Al(PO_4)O, γ-(Zn,Fe)Al(PO_4)O, and $(Mg,Fe)_3(PO_4)_2$ solid solution series. Figure 6 shows a correlation between the mean bond length, d_{mean}, and IS for the trigonal-bipyramidal-coordinated iron site in several phosphates. This tendency corresponds with that for octahedral Fe sites in silicates and oxides. The largest value is shown by the condensed phosphate $Fe_7(P_2O_7)_4$. This was explained (2) by the highly ionic character of the Fe–O bond in diphosphates.

ACKNOWLEDGMENTS

The authors thank Dr. C. A. Geiger for critically reading the manuscript and P. Kluge for help in the preparation of the samples.

REFERENCES

1. Y. Gorbunov, B. Maksimov, Y. Kabalov, A. Ivachenk, O. Melnikov, and N. Belov, *Dokl. Akad. Nauk SSSR* **25,** 785 (1980).
2. B. Malaman, M. Ijjaali, R. Gerardin, G. Venturini, and C. Gleitzer, *Eur. J. Solid State Inorg. Chem.* **29,** 1269 (1992).
3. M. Bouchdoug, A. Courtois, R. Gerardin, J. Steinmetz, and C. Gleitzer, *J. Solid State Chem.* **42,** 149 (1982).
4. D. A. Stephenson and P. B. Moore, *Acta Crystallogr., Sect. B* **24,** 1518 (1968).
5. A. Coda, G. Guiseppetti, C. Tadini, and S. G. Carobbi, *Atti Accad. Naz. Lincei, Cl. Sci.* **8,** 212 (1967).
6. C. Rømming and G. Rade, *Am. Mineral.* **65,** 488 (1980).
7. A. G. Nord and P. Kierkegaard, *Acta Chem. Scand.* **22,** 1466 (1968).
8. E. Kostiner and J. R. Rea, *Inorg. Chem.* **13,** 2876 (1974).
9. E. S. Kostiner, *Am. Mineral.* **57,** 1109 (1972).
10. H. Annersten, T. Ericsson, and A. G. Nord, *J. Phys. Chem. Solids* **41,** 1235 (1980).
11. E. Holland and E. R. Segnit, *J. Aust. Ceram. Soc.* **16,** 17 (1980).
12. L. Cemič and P. Schmid-Beurmann, *Eur. J. Mineral.* **7,** 921 (1995).
13. P. Schmid-Beurmann, L. Cemič, and G. Morteani, *Mineral. Petrol.* **61,** 211 (1997).
14. K.-F. Hesse and L. Cemič, *Z. Kristallogr.* **209,** 660 (1994).
15. K.-F. Hesse and L. Cemič, *Z. Kristallogr.* **209,** 346 (1994).
16. K. Weber, Institut für Mineralogie und Kristallographie, TU Berlin, 1991.
17. F. C. Hawthorne, *Rev. Mineral.* **18,** 255 (1988).
18. K. J. D. MacKenzie and R. H. Meinhold, *Am. Mineral.* **82,** 479 (1997).
19. S. Ghose and T. Tsang, *Am. Mineral.* **58,** 748 (1973).
20. R. Ingalls, *Phys. Rev. A* **133,** 787 (1964).
21. F. Seifert and M. Olesch, *Am. Mineral.* **62,** 547 (1977).
22. J. M. M. Millet, C. Virely, M. Forissier, P. Bussière, and J. C. Vedrine, *Hyperfine Interact.* **46,** 619 (1989).
23. L. Waldrop, *Z. Kristallogr.* **131,** 1 (1970).